Extended laser filamentation in air generated by femtosecond annular Gaussian beams

Z. F. Feng,[1,2] W. Li,[3] C. X. Yu,[1] X. Liu,[3] J. Liu,[1,4] and L. B. Fu[1,4,*]

[1]*National Laboratory of Science and Technology on Computational Physics, Institution of Applied Physics and Computational Mathematics, Beijing 100088, China*

[2]*College of Applied Science, Taiyuan University of Science and Technology, Taiyuan 030024, China*

[3]*China Academy of Space Technology, Beijing Institute of Space Mechanics and Electricity, Beijing 100094, China*

[4]*HEDPS, Center for Applied Physics and Technology, Peking University, Beijing 100871, China and IFSA Collaborative Center of MoE College of Engineering, Peking University, Beijing 100871, China*

(Received 30 January 2015; published 31 March 2015)

Extending the longitudinal range of plasma channels produced by femtosecond annular (ring) Gaussian beams in atmosphere is numerically investigated. We find that the length of a stable plasma channel induced by the annular Gaussian beam, comparing with a Gaussian beam under the same initial condition, has a significant improvement, which can be well understood from two aspects. The dynamic complementation caused by the optical system composing of an axicon and a diverging lens can extend the plasma channel greatly, and the special initial transverse distribution of ring-Gaussian pulse leads to pulse splitting and redistribution of the pulse energy before the formation of optical filament. The ultrashort ring-Gaussian beam perhaps offers a new and an efficient route towards the generation of extended optical filament.

DOI: 10.1103/PhysRevA.91.033839 PACS number(s): 42.65.Re, 42.65.Jx, 52.38.Hb

I. INTRODUCTION

Since Braun *et al.* [1] and others [2] observed the self-guided propagation of intense femtosecond laser pulses in air, the generation of extended plasma channels has attracted much attention for its potential applications in many areas, such as lighting control [3,4], remote sensing of atmospheric pollution [5–7], recognition of distant targets by laser-induced breakdown spectroscopy [8,9], and THz generation [10], etc. Laser filament propagation in air relies on a dynamic balance between Kerr self-focusing, which causes laser intensity to be clamped at a level of $10^{13} \sim 10^{14}$ W/cm^2, and plasma defocusing due to laser-induced ionization with typical peak electron densities limited to 10^{16}–10^{17} cm^{-3}. In this process, a high intensity filament is persisted over many diffraction lengths and leaves in its trail a column of low-density plasma with a lifetime of several nanoseconds [11,12]. Ultimately, the filament vanishes due to the finite energy possessed in the laser pulse, which means an underlying limitation to many practical applications. Therefore, the extension and optimization of optical filament are still desired.

Generally, a single and stable filament can be obtained by using a conventional lens at the cost of decreasing the filament length [13,14], which may reach a few tens of centimeters or even meters. The filament lengths can be extended by simply increasing the input power. However, the incident pulse exceeding the critical power by an order of magnitude will quickly lead to the multifilamentation, which is unstable both in space and time [15]. In previous work, the methods of prolonging approximately twofold elongations have been proposed by varying the shape of input beam, such as using a single-step phase plate [16], or nondiffraction Bessel beams [17–19] . Universally, the Bessel beams are created by Gaussian beams focusing with axicons. Several groups have shown that, the on-axis intensity of axicon-generated beams [20,21] stays high over much longer distances compared to the one focusing with conventional lenses. The nonlinear propagation of axicon-focused beams in air has been theoretically studied in Ref. [22], and they predicted that underdense plasma channels may be created accompanying the beams. Other groups [23,24] have used an axicon to realize laser-generated plasma in argon, which then served as a waveguide for another laser beam. The axicon focusing also become attractive for many nonlinear optical applications, for example, optical coherence tomography [25], optical tweezers [26], and precision laser machining [27], etc. Very recently, Scheller and colleagues report an order of magnitude extension of an optical filament in air by using a secondary low-intensity annular "dressing" beam, which is focused by a conical axicon and continuously refuels the optical filament [28] as a distributed energy reservoir during its propagation. As a promising new approach for generating extended filaments, the utilization of an axicon is very efficient [19–21].

In this paper, we report a new scheme to extend filamentary propagation. We propagate an annular Gaussian beam to pass through an optical system composed of a shallow axicon and a fused silica plano-concave lens. The same set of optical systems for the laser filament has been proposed by the group of Tzortaakis [29], and a considerable increase in the length of the plasma strings has been observed. Here, the main difference is that the laser beam we inject into the nonlinear medium is an axicon-focused annular Gaussian beam. In fact, some nonconventional beam shapes, such as first-order Bessel beams [30], higher order Laguerre-Gauss modes [31] (also called hollow Gaussian beams [32]), Airy beams [33], and optical vortex beams [34], all fall into "annular beams" [35], which refer to any beam with zero center intensity. In recent years, using annular beams, namely hollow Gaussian beams [36] and ring-Airy beams [37], to propagate in the nonlinear medium has been a subject of considerable interest because of their increasing applications in the fields of plasma, atomic, and modern optics [38–41]. Apart from studying these practical applications, here, exploring the fundamental processes for generating ring-Gaussian filament is also very important.

*lbfu@iapcm.ac.cn

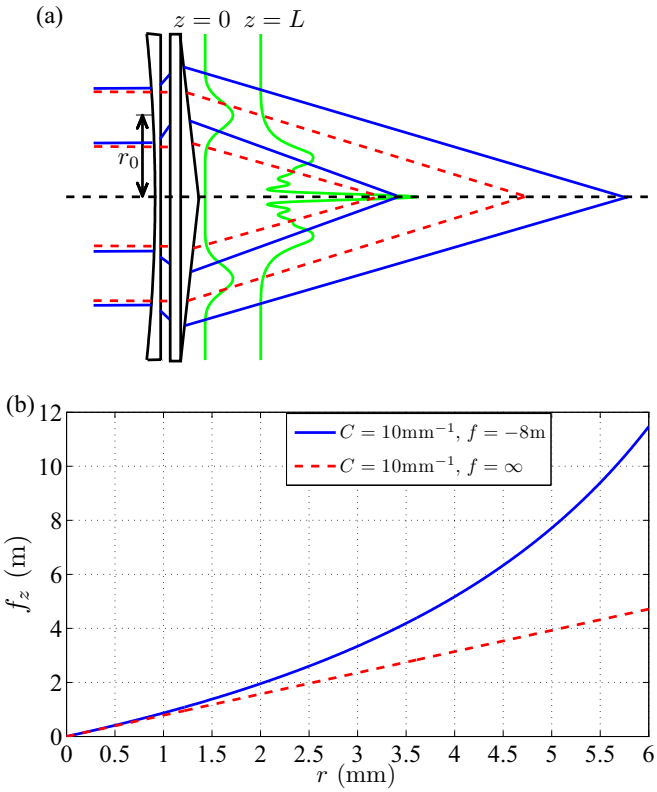

FIG. 1. (Color online) (a) The focusing scheme of an axicon only (red dashed lines) and an axicon preceded by a diverging lens (blue solid lines) for an annular Gaussian beam. Here, r denotes the radius of the ringlike beam. (b) The corresponding axial focusing distance as a function of the transverse radial coordinate.

In the following, we present our scheme and propagation equation in Sec. II. Then in Sec. III, we mainly elaborate the mechanism of the ring-Gaussian filament. Finally, a conclusion is given in Sec. IV.

II. MODEL AND PROPAGATION EQUATIONS

First, we discuss the effect of a conical focusing geometry, as shown schematically in Fig. 1(a). A 40-fs laser pulse at central wavelength $\lambda_0 = 800$ nm with a larger diameter (the radius is r_0) wave front is focused by a set of lens, which is composed of a shallow axicon preceded by a fused silica plano-concave lens. The axicon lens incurs a linear spatial chirp to the annular wave in the transverse plane, which is proportional to $\exp(-iCr)$. Here, C is a phase chirp coefficient and defined by the geometry of the axicon, i.e., $C \approx 2\pi(n - n_0)\alpha/\lambda_0$ (n_0,n are the refractive index of the air and the glass axicon, respectively; α is the base angle of the axicon), and r is the transverse radial coordinate. The introduction of a diverging lens, in fact, changes the base angle of the axicon, which leads to an effective base angle of lens, $\alpha_{\text{eff}} = \alpha + r/[(n - n_0)f]$ (f is the focal distance of the concave). For this optical system, the position of focus displayed in Fig. 1(a) is approximately given by [28,29]

$$f_z(r) = \frac{r}{C/k_0 + r/f}. \tag{1}$$

Here, we omit the thickness of axicon. To guarantee the generation of the laser filament, the values of phase chirp coefficient C and the focal distance of concave f must satisfy $f_z(r) \geq 0$. In this paper, we choose $C = 10\ \text{mm}^{-1}$ and $f = -8$ m. Figure 1(b) shows the axial focus depth as a function of the beam radius. If only the axicon is presented, the axial focus position depends linearly on the beam radius [see the red dashed line in Fig. 1(b)]. While a diverging lens is inserted, the axial focus position f_z is a nonlinear function of beam radius r and the axial focus distance is obviously extended. Moreover, the larger the beam radius is, the greater the extension effect is, as shown in the blue solid line of Fig. 1(b).

The incident pulse is a ring-Gaussian beam with a spatial phase modeling their passage through the concave-axicon,

$$A(r,t,z=0) = A_0 \exp\left[-\frac{(r-r_0)^2}{w_0^2} - \frac{t^2}{\tau_0^2}\right] \times \exp(-iC_{\text{eff}}r), \tag{2}$$

where A_0, w_0, τ_0 are the initial electric field amplitude, e^{-2} beam waist, and the pulse duration, respectively. The effective phase chirp coefficient C_{eff} corresponds to the effective base angle α_{eff}. The initial profile is shown in Fig. 1(a) (at $z = 0$). After propagation over a distance of L, the shape of the transverse mode has changed greatly. Obviously, not only the central core region exhibits strongly nonlinear effects, but also the surrounding annular region will undergo significant self-focusing. It differs from most of the work about Bessel-like beams [19,21,29,42,43], in which nonlinear effects appear only in the intense core, and an external annular region will propagate linearly toward the axis.

To investigate the propagation dynamics of a femtosecond pulse in air, we model the linearly polarized laser electric field with cylindrical symmetry around the propagation axis z in the slowly varying envelope approximation. The evolution of the scalar envelope $A(r,t,z)$ of the electric field can be described by an extended nonlinear Schrödinger (NLS) equation coupled with the laser-plasma production due to multiphoton ionization. The coupled equations in the reference frame moving with the group velocity $v_g = c$ (c is the light speed in vacuum) are written as [44,45]

$$\frac{\partial A}{\partial z} = \frac{i}{2k_0}\nabla_\perp^2 A - i\frac{\beta_2}{2}\frac{\partial^2 A}{\partial t^2} + i\frac{n_2 k_0}{2}|A|^2 A - ik_0\frac{n_e}{2n_c}A - \frac{\beta^{(K)}}{2}|A|^{2K-2}A, \tag{3}$$

$$\frac{\partial n_e}{\partial t} = \sigma_K |A|^{2K}\left(1 - \frac{n_e}{n_{at}}\right), \tag{4}$$

where $\nabla_\perp^2$ is the Laplacian operator and describes transverse diffraction; $k_0 = 2\pi/\lambda_0$ is the central wave number. The second term on the right-hand side of Eq. (3) describes the group velocity dispersion with the coefficient of $\beta_2 = 0.2\ \text{fs}^2/\text{cm}$. The remaining terms account for the self-focusing related to the instantaneous Kerr response with the nonlinear index of refraction $n_2 = 3.2 \times 10^{-19}\ \text{cm}^2/\text{W}$, the plasma defocusing due to the electron with density n_e, and the multiphoton absorption (MPA) with the coefficient of

$\sigma_K = 2.88 \times 10^{-99}$ cm^{2K}/W^K and $\beta^{(K)} = K\hbar\omega_0\sigma_K = 3.1 \times 10^{-98}$ cm^{2K-3}/W^{K-1}, where the number of photons $K = 8$ [44]. In addition, $n_c \approx 1.7 \times 10^{21}$cm^{-3} and $n_{at} = 5.4 \times 10^{18}$ cm^{-3} denote the critical plasma density and the initial neutral atom density, respectively. Here, we neglect the delayed response due to the Raman effect.

III. RESULTS AND DISCUSSION

The numerical scheme of solving the coupled Eqs. (3) and (4) have been performed based on the Fourier and Crank-Nicholson (FCN) method and the split-step spectral methods [45–47]. To start with, the parameters of a ring-Gaussian beam are chosen as follows. The energy of the input pulse is $E_{in} = 5$ mJ, and the pulse duration $\tau_0 = 40$ fs. The width and radius of ring beam are $w_0 = 1$ mm and $r_0 = 3$ mm, respectively.

A. Generation of ring-Gaussian filament

Figure 2(a) shows the spatial distribution of the plasma density (on a logarithmic scale) in the wake of the pulse. The distribution of the energy fluence $F(r,z) = \int_{-\infty}^{\infty} |A(r,t,z)|^2 dt$ is presented in Fig. 2(b), and Fig. 2(c) gives the corresponding on-axis fluence as a function of propagating distance z for the ring-Gaussian beam. It is clear that a stable filament is produced with a length of about 3 m, and the peak electron density reaches $10^{16} \sim 10^{17}$ cm^{-3}. In Fig. 2(b), a pair of yellow lines denote the evolution of the beam radius measured as the half-width at e^{-2} of the fluence distribution along the propagation axis. The nearly constant narrow diameter indicates a stationary filament propagation, which is a standard filamentation feature. It should be noted that although the beam diameter becomes small at a propagation distance between $z = 2.87 \sim 4.5$ m, the filament is not actually formed due to the very low plasma density [see Fig. 2(a)]. This is different from the formation of a conventional Gaussian filament. Since the initial maximal intensity I_0 of the ring-Gaussian beam (at $r = r_0$) is much smaller than that of the Gaussian beam (at $r = 0$) at the same incident energy, beam diameter, and pulse duration, the annular regions contract toward the propagation axis under the action of Kerr self-focusing, which keeps the intensity increasing slowly to 10^{13} W/cm^2, and the corresponding fluence also slowly increases. Meantime, the transverse diffraction is responsible for the rapid disperse of the focusing beams. That is the reason why the distributions of the plasma density [see Fig. 2(a)] and energy fluence [see Fig. 2(b)] have a break, and the on-axis fluence appears a dip [see Fig. 2(c)].

B. The extension effect of a diverging lens

To explore the mechanism of the ring-Gaussian filament and the roles that the lenses play during the laser propagation, we choose several different sets of parameters for lenses. Figures 3(a)–3(c) show the evolution of the maximal laser intensity I_{max}, the peak electron density n_{emax}, and the total energy loss E_{total} for the ring-Gaussian beam ($r_0 \neq 0$) and the Gaussian beam ($r_0 = 0$), respectively. The focal distance of diverging lens $f = \infty$ means an axicon only, and $f = -8$ m represents an axicon accompanying a diverging lens of focal

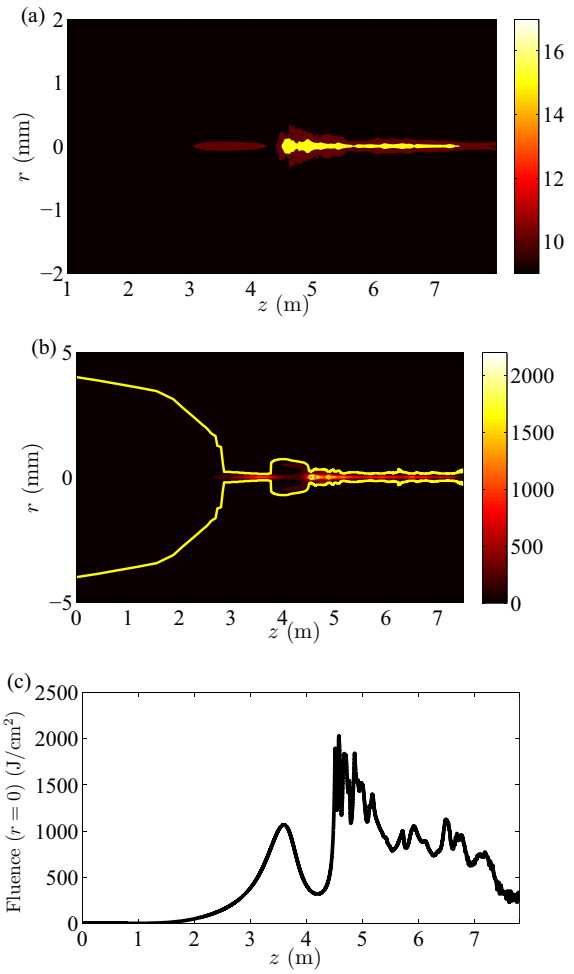

FIG. 2. (Color online) (a) The spatial plasma density (in units of cm^{-3}) distribution on a logarithmic scale with the propagation distance z for ring-Gaussian beam. The input energy is $E_{in} = 5$ mJ, the spatial chirp $C = 10$ mm^{-1}, and the focal distance of concave $f = -8$ m. (b) The energy fluence (in units of J/cm^2) distribution of the laser beam as a function of z and variation of the beam radius at e^{-2} of the fluence distribution is indicated by a pair of yellow lines. (c) The fluence on the axis as a function of z.

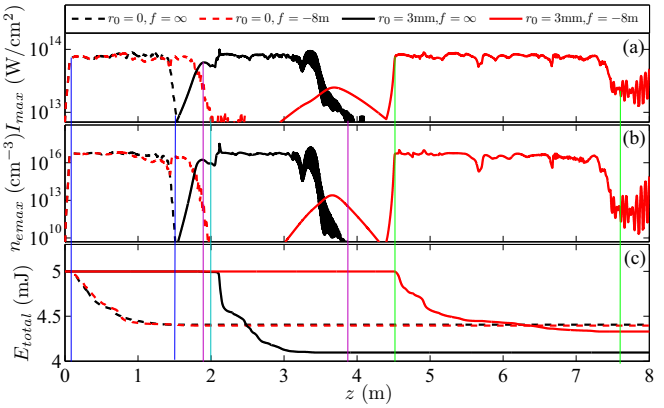

FIG. 3. (Color online) (a) The peak laser intensity. (b) The peak electron density. (c) The energy loss as a function of the propagation distance z for the Gaussian beam ($r_0 = 0$, dashed line) and ring-Gaussian beam ($r_0 = 3$ mm, solid line) with no concave lens ($f = \infty$) (black) and $f = -8$ m (red) under the condition of $C = 10$ mm^{-1}.

distance f, where the spatial chirp induced by the axicon is $C = 10\ \mathrm{mm}^{-1}$. For the incident laser pulse with an e^{-2} beam waist $w_0 = 1$ mm and pulse duration $\tau_0 = 40$ fs, the initial maximal intensity of the Gaussian beam is one order of magnitude larger than that of the ring-Gaussian beam at the same input energy $E_{\mathrm{in}} = 5$ mJ. After propagating only about 0.059 m, the maximal intensity has reached the clamping intensity [11] $I \approx [2n_2 n_c/(\sigma_K t_p n_{\mathrm{at}})]^{1/(K-1)} \approx 5.66 \times 10^{13}\ \mathrm{W/cm^2}$, which is in good agreement with our numerical simulation [the black and the red dashed lines in Fig. 3(a)]. In this case, the laser energy is dissipated very quickly, which means the short filament length (still longer than focused by a conventional lens [21]). Moreover, the extended effect of the diverging lens is not significant, as shown in black and red dashed lines in Figs. 3(a)–3(c).

For the ring-Gaussian beam, the parameters of the optical system are the same as the Gaussian beam, but the cases are noticeably better. First, the filament onset distance is delayed very much, which is mainly due to the decrease of the peak power of the ring-Gaussian beam for the same input energy as the Gaussian beam. When the ringlike beam passes through the concave lens, the filament onset distance is further delayed because the concave lens defocuses the beam, which lowers the beam power [see the black and the red solid lines in Fig. 3]. This means that, in this case, the self-focusing is suppressed and the energy loss is also slowing down, which results in a noticeable extension of the ring-Gaussian filament range. From these figures, we also find that the diverging lens is more sensitive to the ring-Gaussian beam than the Gaussian beam, which is consistent with Fig. 1(b); that is, the larger the beam radius is, the more obvious the expansion of geometrical focusing distance f_z is. In addition, for the ring-Gaussian pulse, its energy decrease of $\Delta E/E_{\mathrm{in}} = 13.4\%$ over about 3 m, which is much slower than the energy drop of $\Delta E/E_{\mathrm{in}} = 12.1\%$ over about 2 m for the Gaussian pulse [see the red solid and dashed lines in Fig. 3(c)]. The slow energy loss allows the ring-Gaussian filament to survive 1.5-fold improvement over the Gaussian filament. Therefore, using the ring-Gaussian beam to generate an extended plasma string is an efficient and viable route.

C. Temporal dynamics of laser filamentation

In order to acquire a deeper insight into the nonlinear dynamics mechanism of the ring-Gaussian filament, we analyze its temporal behavior by comparing with a Gaussian filament. In Figs. 4(a) and 4(b), we present the evolution of the temporal distribution of the on-axis intensity for the ring-Gaussian beam and the Gaussian beam. As shown in Fig. 4(b), the temporal dynamics of the Gaussian beam, which although passing through the combination of the axicon with the diverging lens, still followed the standard spatial replenishment dynamics model. The peak intensity of the front of the pulse increases due to self-focusing, which generates plasmas defocusing to the back of the pulse, and thereby a leading edge is formed ($t < 0$). After the self-focusing collapse, plasmas partly are turned off and the refocusing of the trailing edge ($t > 0$) arouses, which makes the energy refuel the center of the pulse. However, comparing Fig. 4(a) with Fig. 4(b), we find that the main differences between the two pulses are the behaviors before

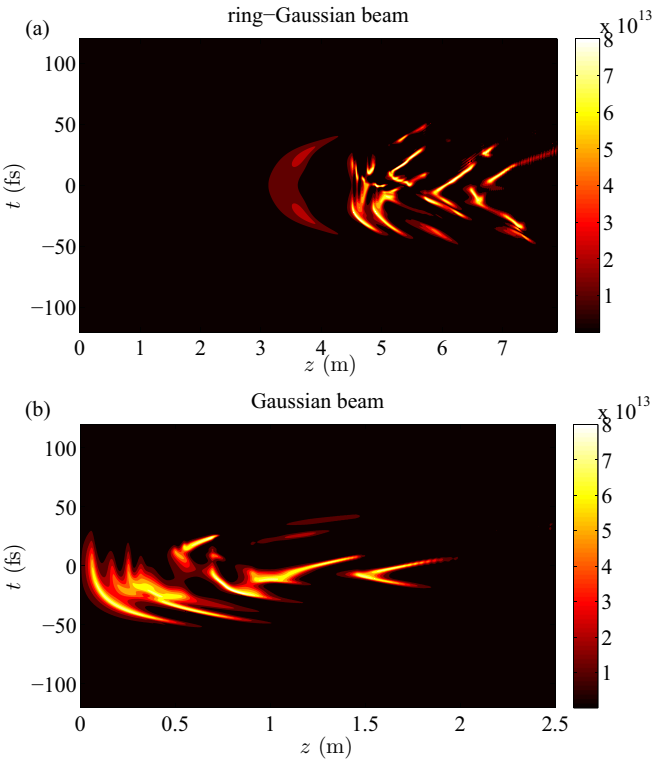

FIG. 4. (Color online) The temporal distribution of the on-axis intensity(in units of $\mathrm{W/cm^2}$) as a function of the propagation distance z for the ring-Gaussian beam (a) and the Gaussian beam (b), the parameters C and f are the same as in Fig. 2.

the formation of the optical filaments. There is a symmetrical shape that appeared for the ring-Gaussian beam, which implies the pulse splitting occurred. Each splitting event leads to a forklike pattern, where the two arms of fork correspond to the leading and trailing split pulses.

For a more detailed analysis of the process before forming the optical filaments, we present the temporal distribution of the on-axis intensity at different propagation distances z for the ring-Gaussian beam and the Gaussian beam in Figs. 5(a) and 5(b), respectively. Clearly, the ring pulse is initially normally distributed in time. After about $z = 3.3$ m of propagation, the pulse begins to split, and two peaks appear symmetrically. Then the time delay between the two peaks becomes larger and larger, while their intensities are decreasing. During laser pulse propagation, another splitting event occurs. However, for the Gaussian pulse, it almost retains its initial shape and only the intensity rises rapidly until the formation of the optical filament. These two different phenomena can be explained by the spatiotemporal intensity distributions of the two laser pulses, as shown in Figs. 5(c) and 5(d). The difference of initial transverse distribution of the two laser pulses leads to different consequences.

For the ring-Gaussian pulse, the initial intensity is Gaussian distributed at the radius of r_0 (here, $r_0 = 3$ mm). Then, due to Kerr self-focusing, the annular wave is gradually contracting to the propagating axis, meanwhile, the central intensity on the axis becomes strong gradually and reaches the maximum when propagating some distances. Of particular interest, the intensity of the external annular region has the same order

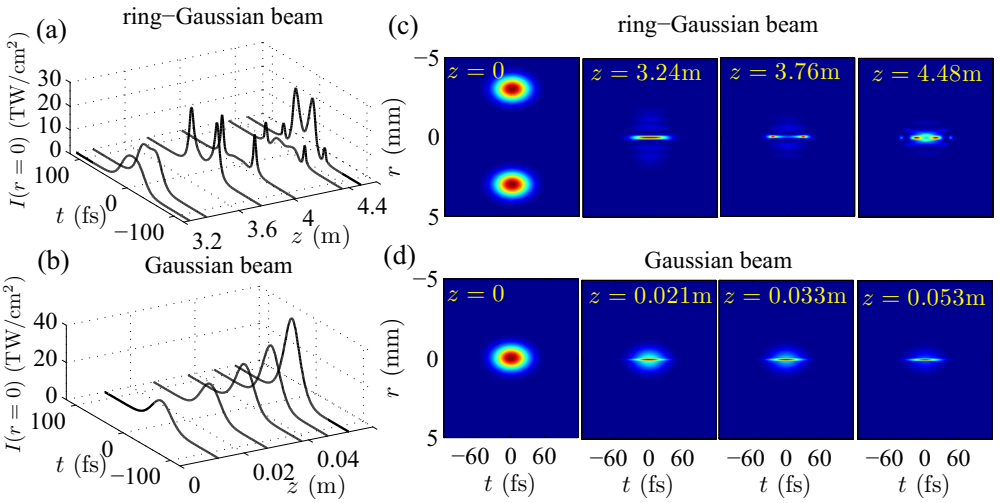

FIG. 5. (Color online) The temporal distribution of the on-axis intensity (a) and (b), and the spatiotemporal intensity distribution (c) and (d) at the different propagation distance z before the formation of optical filament for the ring-Gaussian beam (a) and (c), and the Gaussian beam (b) and (d). The parameters are the same as in Fig. 4.

of magnitude to on-axis intensity, as shown in $z = 3.24$ m of Fig. 5(c). Therefore, the external ring is also sufficient to induce nonlinear self-focusing. Furthermore, at the time ($t = 0$), the pulse is focused faster than the leading and trail edges. While the total energy remains almost constant, hence, on the propagation axis ($r = 0$), the intensity at the time $t = 0$ declines faster than that at the leading and trail edge pulses, which results in the pulse splitting [see $z = 3.76$ m in Figs. 5(a) and 5(c)]. When the energy is again accumulated from annular regions to the central region, the two new split peaks appear as shown in $z = 4.48$ m in Figs. 5(a) and 5(c).

In addition, when an incident Gaussian beam, $A(r,t,z = 0) = A_0 \exp(-r^2/w_0^2 - t^2/\tau_0^2 - iCr)$, passes through an axicon, which in fact generates a Bessel beam, $A(r,t,z_{ax}) \propto J_0(Cr)$, after linear propagation over a distance [22,42]. Here, from the propagation distance $z = 0.021$ m in Fig. 5(d), it is easy to see that the intense central region is surrounded by weaker trails, which is just the characteristics of the Bessel beam. During propagation, the peak of the pulse maintains the strong self-focusing, and nonlinear effects occur within the intense core, thereby an external annular region will only propagate linearly toward the axis, which is the reason for retaining Gaussian shape in Fig. 5(b). Just the difference of propagation characteristics between the two laser pulses before the formation of optical filament leads to the different behavior of laser filamentation.

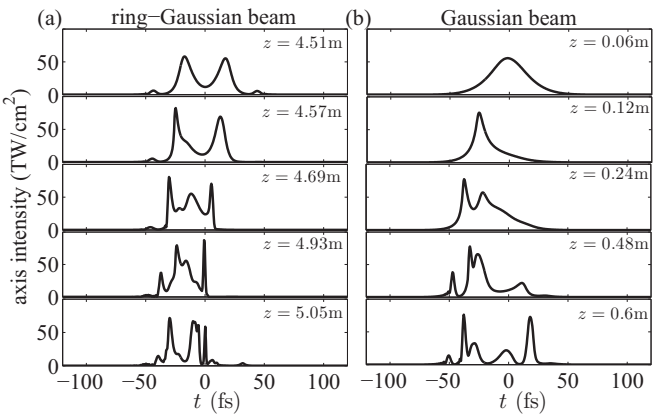

FIG. 6. The temporal distribution of the on-axis intensity at the different propagation distance z after the formation of the optical filament for the ring-Gaussian beam (a) and the Gaussian beam (b). The parameters are the same as used in Fig. 4.

Finally, Fig. 6 shows the temporal distribution of the on-axis intensity for the two types of laser beams at some different distances after the formation of the optical filament. As mentioned above, the filamentation of the Gaussian beam followed the standard spatial replenishment dynamics model. Nevertheless, when the ring-Gaussian beam begins to generate filament, we find that the intensity of the trailing edge of the splitting pulse has a slow decline, and the corresponding intensity of the central region increases, as shown in Fig. 6(a). It implies that there is a gradual energy transport from the trailing edge of the splitting pulse to the central core of the beam during the pulse propagation. So the total energy loss for the ring-Gaussian beam is slow [see Fig. 3(c)]. Furthermore, comparing Fig. 6(a) with 6(b), we can also conclude that the refocusing cycles that the ring-Gaussian filament undergoes is more than the Gaussian filament whenever propagating the equal distance. Therefore, the ring-Gaussian filament is extended a lot, which suggests that the femtosecond annular Gaussian incident beams appear to be better suited for the generation of long plasma channels. We should believe that the length of plasma string can be increased enormously by increasing the input pulse width, power, and adjusting appropriately the parameters of lenses (i.e., phase chirp coefficient C and focal distance of concave f).

IV. CONCLUSION

In conclusion, we have theoretically investigated the characteristics of extended optical filaments generated by the femtosecond annular Gaussian beams in air. The combination

of an axicon with a concave lens can increase the length of the ring-Gaussian filament remarkably comparing with the Gaussian filament under the condition of the same input energy, beam waist, and pulse duration. Furthermore, we find that the modulation effect of the concave lens is more obvious to the ring-Gaussian beam. From the temporal distribution of the on-axis intensity for the ring-Gaussian beam, we observed that the pulse splitting occurs before the formation of the optical filament, which results in a gradual refueling process of laser energy from the trailing edge of the splitting pulse to the central core of the beam, and further leads to multiple refocusing cycles during the filament propagation. It is the main reason that the ring-Gaussian filament is greatly elongated. All of these calculations suggest that the femtosecond annular Gaussian beam can be better suited for the high intensity signal transmission over a long propagation distance and may be a new tool for a broad range of applications, such as remote spectroscopy, THz generation [48], and even in materials processing [35]. In the present experiments, there are many alternative ways to generate annular beams based on the spatial light modulator, aperture, axicons, or a tunable acoustic gradient lens, etc. But using an axicon or a conical lens element is perhaps the most convenient and economical way [35,49].

ACKNOWLEDGMENTS

This work is supported by the National Fundamental Research Program of China (Contracts No. 2013CBA01502, No. 2011CB921503, and No. 2013CB834100), the National Natural Science Foundation of China (Contracts No. 11374040, No. 11274051, and No. 61178067), and a China Postdoctoral Science Foundation funded project (Contract No. 2014M560920).

[1] A. Braun, G. Korn, X. Liu, D. Du, J. Squier, and G. Mourou, Opt. Lett. **20**, 73 (1995).
[2] E. T. J. Nibbering, P. F. Curley, G. Grillon, B. S. Prade, M. A. Franco, F. Salin, and A. Mysyrowicz, Opt. Lett. **21**, 62 (1996); A. Brodeur, C. Y. Chien, F. A. Ilkov, S. L. Chin, O. G. Kosareva, and V. P. Kandidov, *ibid.* **22**, 304 (1997).
[3] S. L. Chin and K. Miyazaki, Jpn. J. Appl. Phys., Part 1 **38**, 2011 (1999).
[4] R. Ackermann, K. Stelmaszcyk, P. Rohwetter, G. Mejean, E. Salmon, J. Yu, J. Kasparian, G. Mechain, V. Bergmann, S. Schaper, B. Weise, T. Kumm, K. Rethmeier, W. Kalkner, L. Wöste, and J. P. Wolf, Appl. Phys. Lett. **85**, 5781 (2004).
[5] P. Rairoux, H. Schillinger, S. Neirdeimer, M. Rodriguez, F. Ronneberger, R. Sauerbrey, B. Stein, D. Waite, C. Wedekind, H. Wille, L. W. Öste, and C. Ziener, Appl. Phys. B **71**, 573 (2000).
[6] J. Kasparian, M. Rodriguez, G. Méjean, J. Yu, E. Salmon, H. Wille, R. Bourayou, S. Frey, Y. B. André, A. Mysyrowicz, R. Sauerbrey, J. P. Wolf, and L. Wöste, Science **301**, 61 (2003).
[7] Q. Luo, H. L. Xu, S. A. Hosseini, J. F. Daigle, F. Théberge, M. Sharifi, and S. L. Chin, Appl. Phys. B **82**, 105 (2006).
[8] K. Stelmaszczyk, P. Rohwetter, G. Méjean, J. Yu, E. Salmon, J. Kasparian, R. Ackermann, J. P. Wolf, and L. Wöste, Appl. Phys. Lett. **85**, 3977 (2004).
[9] H. L. Xu, G. Méjean, W. Liu, Y. Kamali, J. F. Daigle, A. Azarm, P. T. Simard, P. Mathieu, G. Roy, J. R. Simard, and S. L. Chin, Appl. Phys. B **87**, 151 (2007).
[10] C. D'Amico, A. Houard, M. Franco, B. Prade, A. Mysyrowicz, A. Couairon, and V. T. Tikhonchuk, Phys. Rev. Lett. **98**, 235002 (2007); Y. Liu, A. Houard, B. Prade, S. Akturk, A. Mysyrowicz, and V. T. Tikhonchuk, *ibid.* **99**, 135002 (2007).
[11] A. Couairon and A. Mysyrowicz, Phys. Rep. **441**, 47 (2007).
[12] S. L. Chin, S. A. Hosseini, W. Liu, Q. Luo, F. Théberge, N. Aközbek, A. Becker, V. P. Kandidov, O. G. Kosareva, and H. Schroeder, Can. J. Phys. **83**, 863 (2005).
[13] F. Théberge, W. Liu, P. T. Simard, A. Becker, and S. L. Chin, Phys. Rev. E **74**, 036406 (2006).
[14] P. P. Kiran, S. Bagchi, S. R. Krishnan, C. L. Arnold, G. R. Kumar, and A. Couairon, Phys. Rev. A **82**, 013805 (2010).
[15] S. Birkholz, E. T. J. Nibbering, C. Brée, S. Skupin, A. Demircan, G. Genty, and G. Steinmeyer, Phys. Rev. Lett. **111**, 243903 (2013).
[16] Y. Fu, H. Xiong, H. Xu, J. Yao, B. Zeng, W. Chu, Y. Cheng, Z. Xu, W. Liu, and S. Chin, Opt. Lett. **34**, 3752 (2009).
[17] J. Durnin, J. Opt. Soc. Am. A **4**, 651 (1987).
[18] J. Durnin, J. J. Miceli, and J. H. Eberly, Phys. Rev. Lett. **58**, 1499 (1987).
[19] P. Polynkin, M. Kolesik, A. Roberts, D. Faccio, P. D. Trapani, and J. Moloney, Opt. Express **16**, 15733 (2008).
[20] J. H. McLeod, J. Opt. Soc. Am. **44**, 592 (1954); **50**, 166 (1960).
[21] S. Akturk, B. Zhou, M. Franco, A. Couairon, and A. Mysyrowicz, Opt. Commun. **282**, 129 (2009).
[22] D. E. Roskey, M. Kolesik, J. V. Moloney, and E. M. Wright, Opt. Express **15**, 9893 (2007).
[23] C. G. Durfee and H. M. Milchberg, Phys. Rev. Lett. **71**, 2409 (1993).
[24] B. D. Layer, A. York, T. M. Antonsen, S. Varma, Y. H. Chen, and H. M. Milchberg, Phys. Rev. Lett. **99**, 035001 (2007).
[25] Z. Ding, H. Ren, Y. Zhao, J. S. Nelson, and Z. Chen, Opt. Lett. **27**, 243 (2002).
[26] I. Manek, Y. B. Ovchinnikov, and R. Grimm, Opt. Commun. **147**, 67 (1998).
[27] M. Rioux, R. Tremblay, and P. A. Belanger, Appl. Opt. **17**, 1532 (1978).
[28] M. Scheller, M. S. Mills, M. A. Miri, W. Cheng, J. V. Moloney, M. Kolesik, P. Polynkin, and D. N. Christodoulides, Nature Photon. **8**, 297 (2014).
[29] D. Abdollahpour, P. Panagiotopoulos, M. Turconi, O. Jedrkiewicz, D. Faccio, P. Di Trapani, A. Couairon, D. G. Papazoglou, and S. Tzortzakis, Opt. Express **17**, 5052 (2009).
[30] T. Watanabe, M. Fujii, Y. Watanabe, N. Toyama, and Y. Iketaki, Rev. Sci. Instrum. **75**, 5131 (2004).

[31] D. Ganic, X. Gan, M. Gu, M. Hain, S. Somalingam, S. Stankovic, and T. Tschudi, Opt. Lett. **27**, 1351 (2002).
[32] Y. Cai, X. Liu, and Q. Lin, Opt. Lett. **28**, 1084 (2003).
[33] G. A. Siviloglou and D. N. Christodoulides, Opt. Lett. **32**, 979 (2007); G. A. Siviloglou, J. Broky, A. Dogariu, and D. N. Christodoulides, Phys. Rev. Lett. **99**, 213901 (2007).
[34] L. Allen, M. W. Beijersbergen, R. J. C. Spreeuw, and J. P. Woerdman, Phys. Rev. A **45**, 8185 (1992).
[35] M. Duocastella and C. B. Arnold, Laser Photonics Rev. **6**, 607 (2012).
[36] A. Sharma, S. Misra, S. K. Mishra, and I. Kourakis, Phys. Rev. E **87**, 063111 (2013).
[37] P. Panagiotopoulos, D. G. Papazoglou, A. Couairon, and S. Tzortzakis, Nature Commun. **4**, 2622 (2013).
[38] G. Molina-Terriza, J. P. Torres, and L. Torner, Nat. Phys. **3**, 305 (2007).
[39] A. G. York, H. M. Milchberg, J. P. Palastro, and T. M. Antonsen, Phys. Rev. Lett. **100**, 195001 (2008).
[40] N. Blow, Nature (London) **456**, 825 (2008).
[41] V. G. Shvedov, A. V. Rode, Y. V. Izdebskaya, A. S. Desyatnikov, W. Krolikowski, and Y. S. Kivshar, Phys. Rev. Lett. **105**, 118103 (2010).
[42] P. Polesana, M. Franco, A. Couairon, D. Faccio, and P. Di Trapani, Phys. Rev. A **77**, 043814 (2008).
[43] D. Faccio, E. Rubino, A. Lotti, A. Couairon, A. Dubietis, G. Tamošauskas, D. G. Papazoglou, and S. Tzortzakis, Phys. Rev. A **85**, 033829 (2012).
[44] S. Skupin, L. Bergé, U. Peschel, and F. Lederer, Phys. Rev. Lett. **93**, 023901 (2004).
[45] T. T. Xi, X. Lu, and J. Zhang, Phys. Rev. Lett. **96**, 025003 (2006).
[46] P. Sprangle, J. R. Peñano, and B. Hafizi, Phys. Rev. E **66**, 046418 (2002).
[47] G. P. Agrawal, *Nonlinear Fiber Optics* (Academic Press, San Diego, 1995).
[48] S. Hussain, M. Singh, R. K. Singh, and R. P. Sharma, Europhys. Lett. **107**, 65002 (2014).
[49] J. A. Gemmera, S. C. Venkataramani, C. G. Durfee, and J. V. Moloney, Physica D **283**, 15 (2014).